Received: 27 September 2024 | Revised: 6 June 2025 | Accepted: 18 August 2025

DOI: 10.1002/esp.70150

RESEARCH ARTICLE

ESPL WILEY

Predicting rainfall kinetic energy under forest canopies—*A pilot study using ULS*

Johannes Antenor Senn[1] | Jannika Schäfer[1] | Zahra Hosseini[1,2] | Steffen Seitz[3]

[1]Institute for Geography and Geoecology, Karlsruhe Institute of Technology, Karlsruhe, Germany

[2]Department of Forestry, Faculty of Agricultural and Natural Resources, Lorestan University, Khorramabad, Iran

[3]Department of Geosciences, University of Tübingen, Tübingen, Germany

Correspondence
Johannes Antenor Senn, Institute for Geography and Geoecology, Karlsruhe Institute of Technology, Karlsruhe, Germany.
Email: senn@kit.edu

Funding information
This research received no specific grant from any funding agency in the public, commercial, or not-for-profit sectors.

Abstract

Rainfall erosivity, expressed in kinetic energy, is determined by intensity, velocity and drop size distribution. In natural precipitation, these properties vary and can be substantially altered by the vegetation before reaching the ground. The splash effect of impacting raindrops on the soil surface can initiate soil erosion. While research in this regard has focussed on relating plant characteristics to erosion processes, there is a lack of studies that attempt to reverse this by predicting throughfall kinetic energy from plant properties. This has been attempted by the Vegetation Splash Factor (VSF), a model solely based on the three-dimensional distribution of vegetation surfaces derived from forest lidar forest data. We conducted a pilot study using the VSF model to validate it with in situ measurements and confirm its general suitability. We found a significant correlation between the observed and predicted effect of vegetation on the kinetic energy of rainfall, which demonstrates the suitability of the VSF, despite being solely based on structural traits. The observed effect of vegetation on rainfall kinetic energy exceeded literature reports, leading to systematic underestimation by the model. Our results showed that the VSF can be used to spatially continuously predict the effect of vegetation on the erosivity of rainfall from high-resolution lidar data. These findings open new possibilities for research on splash erosion under vegetation, shifting the perspective from point-based studies towards area-wide approaches. The simplicity of the approach facilitates adaptation for wider use. The first application of the VSF in a field study has proved that the concept is functional and can illustrate zones of increased potential for soil loss under full vegetation cover. This adds to the methodological tool box for erosion studies and can support decision-makers in forestry and agriculture in the future.

1 | INTRODUCTION

Water erosion is a significant landscape-shaping factor and a major cause of global soil degradation (Scholten & Seitz, 2019). The economic damage to agricultural land caused by soil loss has been the focus of erosion research for decades. However, it is less widely recognised that erosion processes also occur under the closed canopies of natural and managed forests worldwide (Gall et al., 2022; Zemke, 2016). Despite extensive research on erosion, individual mechanisms such as the splash effect are still not thoroughly explored (Goebes et al., 2014). The splash effect refers to the kinetic impact of raindrops on the soil surface that can initiate water erosion. The kinetic energy (KE) applied to the soil increases with the mass and velocity of a drop (Ellison, 1948b). Within nature-like drop sizes and a terminal velocity of 9 m s^{-1}, pressures between 2 and 6 MPa can be achieved during the 50 ms of drop impact (Ghadiri & Payne, 1981, 1986; Marzen & Iserloh, 2021). This energy weakens and fragments soil aggregates and can move particles over distances of several decimeters depending on the kinetic energy and substrate (Marzen & Iserloh, 2021; Van Dijk, Meesters, & Bruijnzeel, 2002). The loosened material is susceptible to subsequent transport by surface runoff, which sets in once the soil reaches infiltration capacity (Morgan, 2005).

The magnitude of the splash effect is determined by the erosivity of rainfall—which is the focus of this study—and the erodibility of the soil surface. The erosivity induced by the KE of rainfall is determined by the velocity and Drop Size Distribution (DSD), which characterises the drop spectrum based on the frequency of drops per size. Numerous studies have shown that the DSD differs significantly between freefall (no intermediate interception) and stand precipitation (throughfall) (Calder, 1996; Dunkerley, 2020; Geißler et al., 2012; Katayama et al., 2023). Plant surfaces intercept freefall precipitation, temporarily retain it and then release it through evaporation, stemflow or throughfall precipitation (Levia et al., 2019). Previous research has investigated this effect of vegetation on DSD by species-specific traits and found that the most influential variables are height and width of canopies, size and shape of leaves, leaf margins, branch angles and the height of the first branch (Geißler et al., 2012; Goebes et al., 2015a; Herwitz, 1987; Nanko et al., 2008). Finally, the throughfall kinetic energy (TKE) can differ substantially from the initial freefall kinetic energy (FKE) (Nanko, Hotta, & Suzuki, 2006). This is because heavy drops released from high canopy layers can gain high velocities and thus high KE on impact. However, when drops are re-intercepted by lower vegetation layers, they disperse into tiny droplets (Levia et al., 2017; Nanko et al., 2008; Nanko, Hotta, & Suzuki, 2006; Nanko, Hudson, & Levia, 2016). Because of this dispersion effect and the lack of sufficient falling height for drops accumulated on the surfaces of low vegetation layers, understoreys can reduce the TKE and thus provide a protective effect (Calder, 2001; Chapman, 1948; Katayama et al., 2023). As a result, the TKE can significantly deviate from the FKE, which varies depending on the vegetation properties (Geißler et al., 2012; Nanko, Hotta, & Suzuki, 2004; Song et al., 2018). The ratio between TKE and FKE quantifies this effect of vegetation on the KE of rainfall (Goebes et al., 2015b). However, increased sediment discharge under vegetation depends above all on soil erodibility. Besides soil properties, erodibility is controlled by the percentage and properties of the soil cover consisting, for example, of leaf and needle litter or biological soil crusts (Lacombe et al., 2018; Liu et al., 2017; Miura et al., 2015; Seitz et al., 2017). Disturbance or absence of such a protective layer can result in significant soil degradation if DSDs are correspondingly erosion-promoting (Abe et al., 2024; Gall et al., 2022; Seitz et al., 2016).

More recent studies have focussed on measuring plant characteristics and their impact on erosivity. These studies have often focussed on plantations because their homogeneous vegetation structure makes them particularly susceptible to erosion. Based on different subsets of plant traits, these studies have investigated plantations of, for example, banana (Ji et al., 2022; Zhang et al., 2021), rubber (Liu et al., 2018), olives (Beniaich et al., 2022), corn and soybean (Ma et al., 2015). Studies have also considered the effect of strategic intercropping to reduce TKE through ground cover (Beniaich et al., 2022; Lacombe et al., 2018; Liu et al., 2018). Other studies have investigated TKE under urban trees (Alivio, Bezak, & Mikoš, 2023), gradually modified single trees (Nanko et al., 2008) and under forest stands of different levels of species diversity (Goebes et al., 2015b). The studies mentioned highlight the need for more comprehensive data and recommend expanding existing datasets to include additional ecosystems and vegetation zones (Fernández-Raga et al., 2017; Goebes et al., 2016; Levia et al., 2019). We found that there is a need for comparability of datasets and standardised methods for vegetation mapping.

One reason for the lack of data is that the high workload of methodologies used limits the scalability of research in this area (see Fernández-Raga et al. [2017] for an overview of methods). A method to measure rainfall KE that has been tried and tested for decades are splash cups (Ellison, 1948a; Fernández-Raga et al., 2019). These sand-filled cups are installed on site during and after the rainfall event. KE can be estimated from sand loss via a linear function. The Tübingen splash cup (T-cup) was developed by Scholten et al. (2011) for KE measurements with high replication and has been widely adopted as cost-effective means to investigate the effect of plant traits, for example, by Geißler et al. (2012), Goebes et al. (2015b) and Shinohara et al. (2018). Alternatively, laser disdrometers or acoustic sensors that directly record and analyse drop spectra electronically can be employed, although the cost per unit prevents application in large numbers (Angulo-Martínez et al., 2018; Johannsen et al., 2020). The measurement methods mentioned share a point-based labour intensive nature, which limits their ability to spatially continuously capture the entire landscapes or forests.

In contrast, area-wide mapping of vegetation traits using active and passive remote sensing methods is well-established. Data from airborne and spaceborne sensors have become a fundamental resource in the biogeosciences over the last two decades (Boyd & Foody, 2011; Lechner, Foody, & Boyd, 2020). TKE-relevant vegetation traits such as leaf area index (LAI) or chlorophyllous content can be derived from the spectral signal using radiative transfer modelling (Cherif et al., 2023; Kattenborn, Fassnacht, & Schmidtlein, 2019), aggregated from look-up tables after species classification or directly determined from high-resolution scenes using image recognition, for example, leaf angle (Kattenborn et al., 2022). In recent years, we have seen significant progress in the field of digital vegetation mapping using both terrestrial laser scanning (TLS) and airborne laser scanning (ALS) (Åkerblom & Kaitaniemi, 2021; Hyyppä et al., 2020). The key advantage of lidar is that vegetation structure is captured directly in 3D. The use of individual tree point clouds and tree measurements from multi-platform laser scanning for forest vegetation inventories has been successfully demonstrated by, for example, Schneider et al. (2019) for tropical and temperate forests. Lidar applications have been used to describe forest–water interactions such as throughfall partitioning modelling (Schumacher & Christiansen, 2020). These approaches have led to new insights, such as the fact that smaller trees are more efficient in producing stem flow (Exler & Moore, 2022). Furthermore, lidar can be used to directly estimate vegetation structure per grid cell such as LAI (Morsdorf et al., 2006), fractional vegetation cover (FVC) (Xu et al., 2019) or per voxel, for example, leaf area density (LAD) (Gonsamo, D'odorico, & Pellikka, 2013) and gap fraction (Bouvier et al., 2015). Finally, lidar can also be used to directly estimate vegetation traits such as leaf angle (Itakura & Hosoi, 2019; Liu et al., 2019). These spatially continuous vegetation datasets provide valuable information that can be linked to erosion potential.

Erosion research and silvicultural management have a great need for large-scale estimates of the effect of vegetation on the erosivity of rainfall (Beniaich et al., 2022). As part of the widely used erosion model RUSLE, a crop factor was assigned according to land cover categories (Panagos et al., 2015). Numerous studies have investigated erosion by measuring soil loss, for example, using runoff plots or sediment yields (Zhang et al., 2014). Direct remote sensing-based mapping

of erosion patterns and moving sediment volumes has been used for a long time (Sepuru & Dube, 2018; Vrieling, 2006). However, in studies focussing on erosion, the rainfall erosivity cannot be separated from the soil erodibility (Zhang et al., 2014). Therefore, these data are not suitable to investigate TKE. There are few approaches that allow large-scale calculation of potential erosion from digitally recorded vegetation data (Zhongming et al., 2010). Usually, these approaches focus on the protective effect of vegetation and ignore the potential to increase the TKE. Previous remote sensing-based approaches have directly related erosion to the condition of the crowns and gaps in the canopy (Xu et al., 2019; Zhang et al., 2014); however, the possibility that closed canopies within vital forest vegetation can increase sediment discharge was again neglected.

Most TKE research to date has focussed on observing TKE and the plant characteristics that influence its magnitude. However, to our knowledge, hardly any study made the attempt to reverse this mechanism and predict TKE locally from plant characteristics; an approach that becomes even more promising with the availability of spatially continuous vegetation data. Senn et al. (2020) have thus proposed an approach for the area-wide prediction of the effect of vegetation on TKE: the Vegetation Splash Factor (VSF). The conceptual model applies point clouds from aerial lidar (uncrewed laser scanning [ULS] or ALS) to map vegetation structure in a 3D voxel space. The model attributes amplifying and protective effects to the voxels based on the vertical distribution of gaps and vegetation cover. The calculated VSF maps indicate the predicted modifications of the KE relative to open rainfall (Senn et al., 2020). The modelled VSF values are consequently analogue to the observed TKE/FKE-ratios from in situ measurements. However, a practical evaluation and application using in situ KE measurements was still pending so far. Therefore, we aimed to adapt the VSF concept in a temperate deciduous forest study area in south-west Germany using a ULS dataset to test the initial concept with minimum modifications. Thus, we addressed the following research questions:

1. Do the observed TKE/FKE ratios correspond to those reported in the literature?
2. Do the spatial patterns of VSF values agree with the vegetation structure?
3. Do the observed TKE/FKE ratios correspond to the VSF values?
4. Can the VSF be used to predict the erosivity of rainfall?

2 | METHODS

To address our research questions, we acquired a ULS dataset of a forested study area to calculate the VSF map. We equipped the field site with four transects of splash cups to measure the KE of rainfall.

2.1 | Experimental design and study area

The research area is located in a mixed broad-leaved forest near Bretten, Germany (49.01576°N, 8.68464°E) at 180 m a.s.l. (Figure 1). The climate is temperate, warm and classified as Cfb according to Köppen–Geiger (DWD, 2024). The average annual temperature is

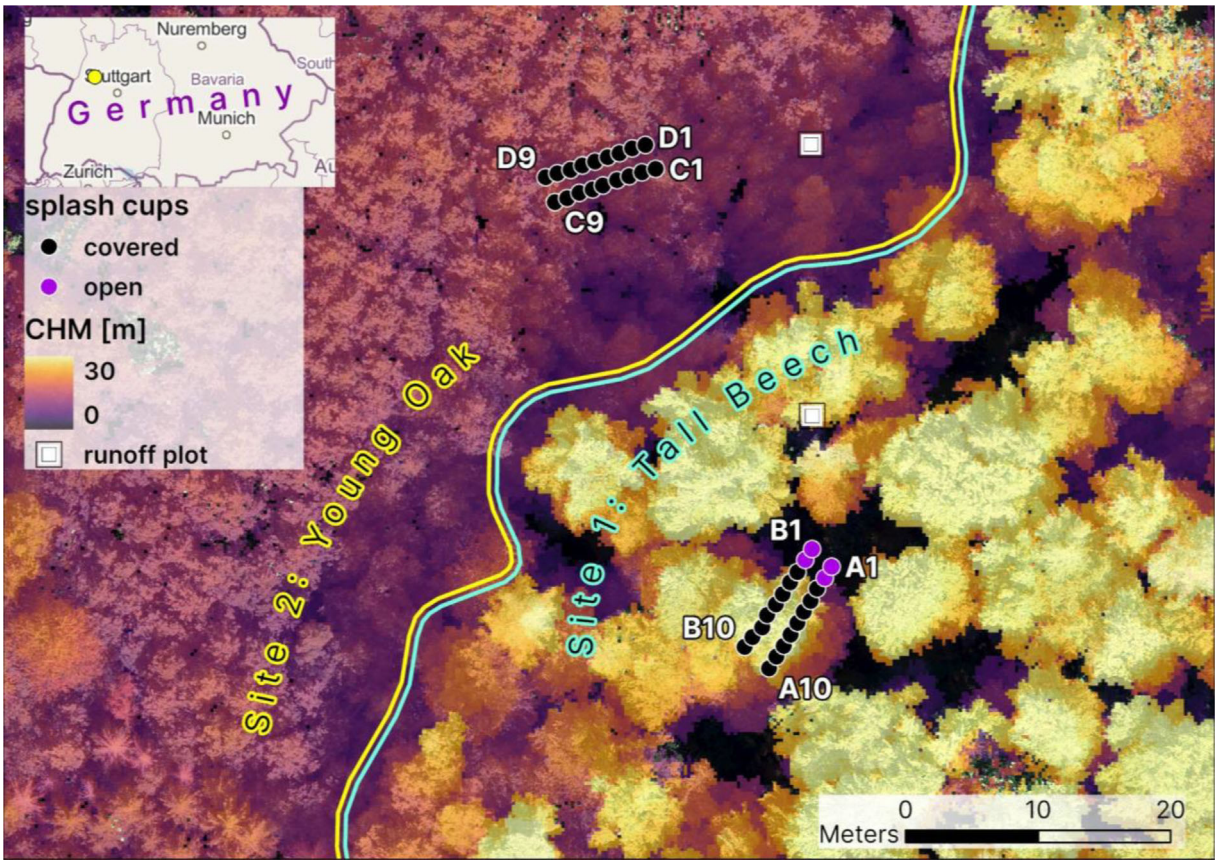

FIGURE 1 Map and orthophoto of the study area, overlaid with the canopy height model (CHM) and the splash cup positions. The circles indicate the cup positions and are not to scale.

FIGURE 2 Measurement transects and vegetation on Site 1 (a) and Site 2 (b) with an exemplary splash cup before a rainfall event (c) and after a rainfall event without forest canopy (d: FKE) and with closed forest canopy (e: TKE).

10.8°C, with an annual precipitation of 909 mm (German Meteorological Service, weather station #710 'Bretten', DWD, 2024).

We defined the study area to include two stands with distinctly different vegetation structures, which will be referred to as Site 1 and Site 2 (Figure 1). At each site, we established two parallel transects to measure the KE of rainfall. The first site (transects **A** and **B**) was dominated by large individual beech trees (*Fagus sylvatica*) with a diameter at breast height (DBH) of approximately 45 cm and a height of 30 m. These trees had large crowns accompanied by some smaller understorey elements (Figure 2a). We installed these two transects to cover a gradient from dense canopy cover to freefall conditions. The transects run parallel to a gravel track that crosses the site and is mostly covered by overhanging canopy. The second site (transects **C** and **D**) was characterised by a young and dense oak tree stand (*Quercus robur*) with a DBH of approximately 20 cm and a height of 16 m. Because this stand was a plantation with fixed row spacing, there was little variation in terms of tree heights and featured only few canopy openings (Figures 1 and 2b).

Previous investigations using micro-scale runoff plots (40 cm × 40 cm) indicated slightly accelerated soil erosion during heavy rainfall events in zones without soil cover caused by surface disturbance through walkover. We measured sediment transport rates of 17.5 g m^{-2} on bare ground compared to <1 g m^{-2} with leaf litter cover for Site 1, and 9.5 g m^{-2} on bare ground and <0.1 g m^{-2} with moss-dominated biocrust cover on Site 2. Moreover, we observed small rills near the tree stems and on runoff plots with bare ground.

2.2 | KE measurements with splash cups

We applied T-cups (Scholten et al., 2011) to measure sand loss as a proxy for KE (Figure 2). The splash cups were filled with standardised unit sand (125–200 µm particle size) and deployed on a carrier system in the field (Figure 2c). Sand loss was determined from the difference in dry weight of the prepared splash cups before and after a major rainfall event. Subsequently, we derived the KE from the sand loss using a linear regression function calibrated with a laser disdrometer (Scholten et al., 2011). The cups were mounted on bamboo sticks, 15 cm above the ground and distributed along transects with 1-m spacing. Ten splash cups each were installed for transects **A** and **B**, and nine splash cups were installed each for transects **C** and **D** (Figure 1), resulting in a total of 38 measurements per time step.

We georeferenced the cup locations using relative positions from a TLS scan registered to the ULS dataset. Splash cup measurements were carried out at six timesteps between July and October 2020, with cups collected after significant precipitation events or a maximum of 4 weeks in the field (Table 1). Precipitation totals and event peaks defined as maximum intensity during an erosive rainfall event were retrieved from the DWD (2024) for each time step. T-cups were closely monitored to avoid rim effects (Scholten et al., 2011). Wind effects were not observed because of the constant moisture penetration in T-cups under wind-breaking tree vegetation. Wildlife damage occurred sporadically and the corresponding cups were discarded. Thus, the T-cup measurements have proven to be reliable.

2.3 | Remote sensing measurements

We conducted the ULS scans in August and September 2019 using a RIEGL miniVUX-1UAV (Riegl Laser Measurement Systems GmbH, Horn, Austria), installed on a DJI Matrice 600 Pro (DJI Ltd., Shenzhen, PR China) uncrewed aerial vehicle (UAV). The UAV travelled at a speed of approximately 5 m s^{-1} at an altitude above ground of approximately 60–80 m using a pulse repetition frequency of 100 kHz and a scan frequency of 50 lines per second. We used scan angles of ±90°. The ULS acquisitions were conducted with two overlapping double grids with a spacing between the scan lines of 26–30 m. This combination of settings led to a point cloud density of approximately 800–1200 points m^{-2} (see Weiser et al., 2021). Two additional sets of co-registered ground-based TLS scans were acquired on the 28th September 2020 during the survey period. From these high-resolution TLS point clouds, we manually extracted the exact positions of the splash cups. We found the resulting positional accuracy to be superior over differential Global Navigation Satellite System (GNSS) measurements performed under the tree canopy.

2.4 | Calculating the VSF

We applied the acquired ULS point cloud to calculate the VSF as described by Senn et al. (2020). The underlying conceptual model is shown in Figure 3. The model simulates the movement of raindrops falling through the canopy based on the three-dimensional distribution of vegetation surfaces to estimate how the KE of rainfall is modified.

As a first step, we estimated the vegetation cover in a three-dimensional voxel space (transparent column in Figure 3a) using modified functions from the lidR R package (Roussel et al., 2020; Roussel & Auty, 2024). The proportion of horizontal ground coverage by vegetation can be quantified as vegetation cover and its counterpart, the gap fraction. It is 'the proportion of horizontal vegetated area occupied by the vertical projection of canopy elements' (Gonsamo, D'odorico, & Pellikka, 2013). To translate this into a three-dimensional representation of the distribution of vegetation surfaces, the gap fraction can be divided into vertical increments called the gap fraction profile. This procedure is visualised by an exemplary column of voxels over a grid cell in Figure 3. We calculated the gap fraction profile using 25-cm increments on a 50-cm grid, representing an increase in

TABLE 1 Overview of the observations. The sampled timesteps with precipitation events (DWD 2020), mean sand loss and kinetic energies measured and normalised by rainfall amount.

Time step	Start	End	Precipitation [mm]		Mean sand loss (g)	Mean KE (J m^{-2})	FKE (J m^{-2})	Mean TKE [J m^{-2}]			TKE/FKE ratio			Normalised		
			Total	Daily peak				All	Site 1	Site 2	All	Site 1	Site 2	Mean KE (J m^{-2} mm)	TKE (J m^{-2} mm^{-1})	FKE (J m^{-2} mm^{-1})
a	07.07.	21.07.	23.0	14.4	3.65	319.25	44.17	353.63	234.00	459.18	8.01	5.30	10.40	13.88	15.38	1.92
b	21.07.	05.08.	2.8	2.4	0.55	48.07	29.50	50.32	24.27	74.84	1.71	0.82	2.54	17.17	17.97	10.54
c	05.08.	26.08.	25.9	15.5	5.97	522.82	159.25	566.89	545.63	586.91	3.56	3.43	3.69	20.19	21.89	6.15
d	26.08.	18.09.	21.5	13.1	3.66	320.17	68.07	353.78	216.19	474.17	5.20	3.18	6.97	14.89	16.45	3.17
e	18.09.	28.09.	39.5	19.5	7.17	627.80	254.86	674.42	529.60	802.20	2.65	2.08	3.15	15.89	17.07	6.45
f	28.09.	22.10.	22.1	3.4	3.61	315.98	76.74	347.59	237.85	473.00	4.53	3.10	6.16	14.30	15.73	3.47

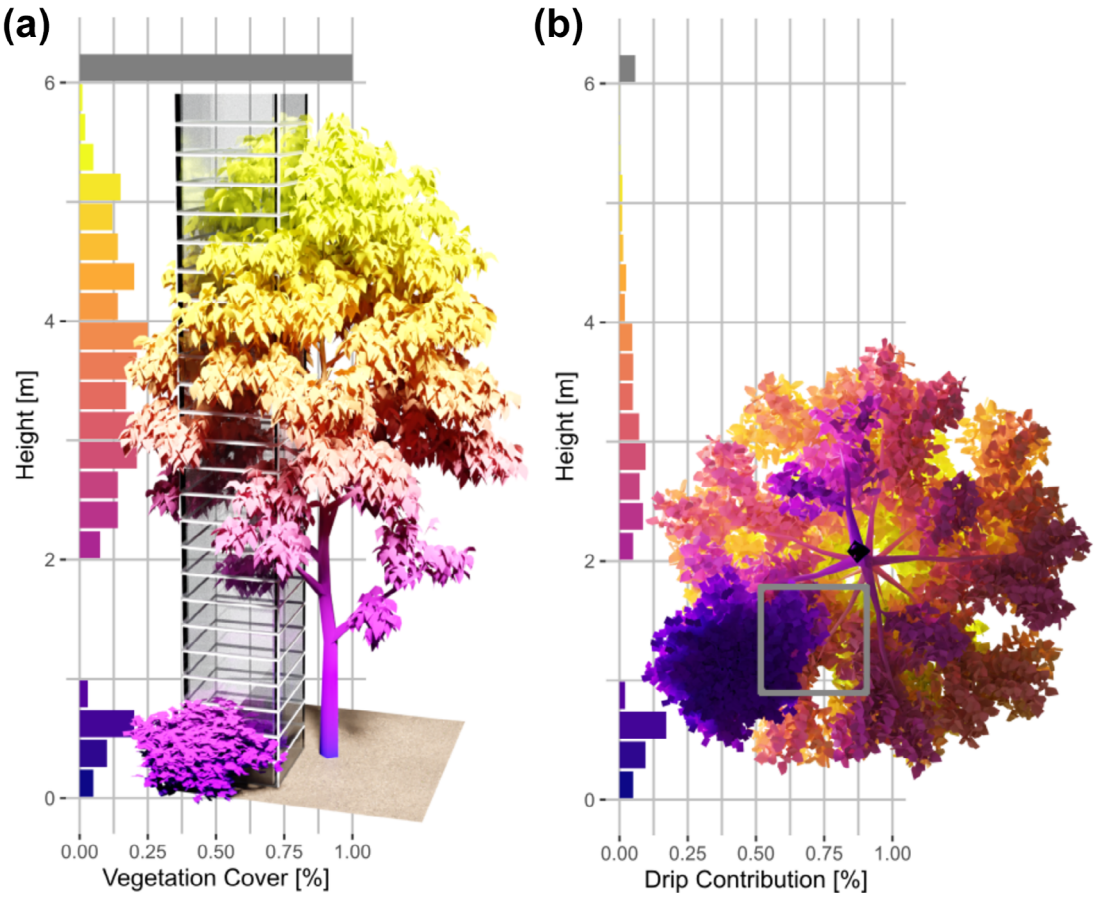

FIGURE 3 Visualisation of the vegetation splash factor concept in an exemplary vegetation plot viewed from the (a) side and the (b) bottom coloured by height. An exemplary grid cell is visualised (a) as a column vertically sectioned into voxels to illustrate how the vegetation cover per voxel translates into a corresponding histogram. The same grid cell viewed from the bottom up (b) illustrates the surface fractions visible from the ground and thus contributing drops to the bare ground. The histograms demonstrate how the vegetation cover of the voxel cells (a) translates into the drip contribution (b).

spatial resolution compared to the design used by Senn et al. (2020), who used 1-m increments on a 5-m grid. This adaptation was both possible and necessary because of the higher spatial resolution of the lidar dataset.

In the second step, we calculated the drip contribution. This metric indicates the percentage of area per voxel from which drips reach the ground without further interception. This can be imagined as a projection of surfaces visible from the ground (cf. Figure 3b). Thus, the sum of the drip contribution for each cell is 1. In the case of incomplete vegetation cover, the proportion of uncovered ground surface is attributed to the open throughfall (grey bar).

In the third step, we transformed the drip contribution values with a height-dependent weighting factor to account for the protective or amplifying effect of each vertical increment. Starting with 0.5 (protective) at ground level, it increases to 1 (neutral) at 1 m, then rises steeply at first and slowly approaches its maximum of 3 up to a height of 10 m, from where drops of all sizes can reach their terminal velocities (Gunn & Kinzer, 1949; Serio, Carollo, & Ferro, 2019). The dimensions of the protective and amplifying effect are based on TKE/FKE-ratios from the literature (e.g. Foot & Morgan, 2005; Geißler et al., 2013; Goebes et al., 2015b; Nanko et al., 2008) and are explained in more detail by Senn et al. (2020). Finally, we calculated the VSF by vertically integrating the weighted drip contribution values over each grid cell.

2.5 | TKE prediction

The VSF was designed to reflect the protective or amplifying effect of vegetation on TKE relative to FKE (Senn et al., 2020). Conversely, we assume that TKE can be predicted based on the observed FKE measured by the splash cups under open canopy positions. For each timestep, we calculated the FKE baseline by averaging the measurements of the four freefall cups. We then multiplied the VSF raster with these FKE baseline values to spatially predict TKE. The TKE prediction is therefore a linear scaling of the VSF as a function of the observed erosivity of the open precipitation.

3 | RESULTS

The precipitation dataset provided by the German Weather Service (DWD, 2024) showed six relevant events during the survey period (Table 1). Four of the recorded rainfall events (**a, c, d, f**) had similar total precipitation volumes of about 23 mm. Events **b** (2.8 mm) and **e** (39 mm) showed more extreme values.

We collected 228 valid splash cup measurements over the study period. For each timestep, we calculated the TKE from the sand loss observations measured at the cups (Table A1). The results showed an

average sand loss of 4.1 g, corresponding to an average KE of 359 J m^{-2} across all measurements (Table 1).

We calculated an average ratio of 4.28 between FKE and TKE, indicating an overall increase in rainfall KE from the passage through the vegetation (Table 1). The smallest TKE/FKE ratios occurred at timesteps **b** (1.71) and **e** (2.65) (min and max precipitation), while we observed the highest ratio at timestep **a** (8.01). On average, the TKE/FKE ratios were 2.99 (Site 1) and 5.49 (Site 2).

The splash cup TKE observations along the four transects are visualised as black points (purple for FKE) in the bottom panel of Figure 4, arranged vertically according to the six timesteps. The TKE predictions are visualised as black lines on top of the corresponding observations and will be further described in Section 3.2.

The extremes in the observed TKE values coincide with the extremes in the precipitation records, that is, low in timestep **b** and high in timestep **e**. Site 2 resulted in systematically higher values with a smaller variation. The KE varied with position class, and we measured the lowest values at the FKE cups. We measured a mean FKE of 298 J m^{-2} at Site 1 and 478.3 J m^{-2} at Site 2. On average, the erosivity under the young oaks (Site 2) was twice as high as under the large beech stand (Site 1). In addition, we have observed higher standard deviations of KE measurements per timestep on Site 1.

The top panel of Figure 4 shows four transects through the vegetation cover voxel space. These profiles can be directly related to the TKE observations. The graphs suggest that high values coincide with tall canopies and long falling heights, especially on Site 2. Low VSF values can be found in cells with overall low vegetation cover or predominantly low vegetation. The vegetation cover profiles show a higher overall number of voxel cells containing vegetation on Site 1 (transects **A** and **B**, tall beech trees). Although Site 1 has a denser understorey than Site 2 (transects **C** and **D**, young oak trees), this difference is not reflected in the canopy cover profile.

3.1 | VSF estimation: Predicted effect of vegetation on rainfall erosivity

We calculated the VSF with a resolution of 0.5 m for an area of 100 × 100 m that contains the two sites. The resulting raster is shown in Figure 5 with an overlay of the cup positions and the buffers created to analyse the characteristics of the two sites. Statistical metrics of the entire study area and the buffers around the transects can be found in Table 2. Over the entire survey area, 0.12% cells contained NAs, 74.8% of the cells contained values above 1, and the values ranged from 0.27 to 2.98 with a mean of 1.47.

The characteristics of the two sites—stratified by dominant age, structure and species—are reflected in the calculated VSF values. Site 1, featured tall beech trees with a medium-dense understorey and resulted in a heterogeneous spatial pattern of VSF values. VSF values below 1 coincided with gaps in the canopy, whereas the dense crowns resulted in high values above 2. The young oak trees at Site 2, in contrast, resulted in a more homogeneous distribution of VSF values. A gravel track running through Site 1 can be recognised in the VSF raster (dashed line in Figure 5). It is characterised by extremely high VSF values where there are overhanging canopies and low values under gaps.

To further characterise the two sites, we extracted the VSF values using a 10-m buffer around the cup locations. The statistical metrics for the buffer areas are presented in Table 2, with the corresponding histogram shown in Figure 6. The mean values suggest

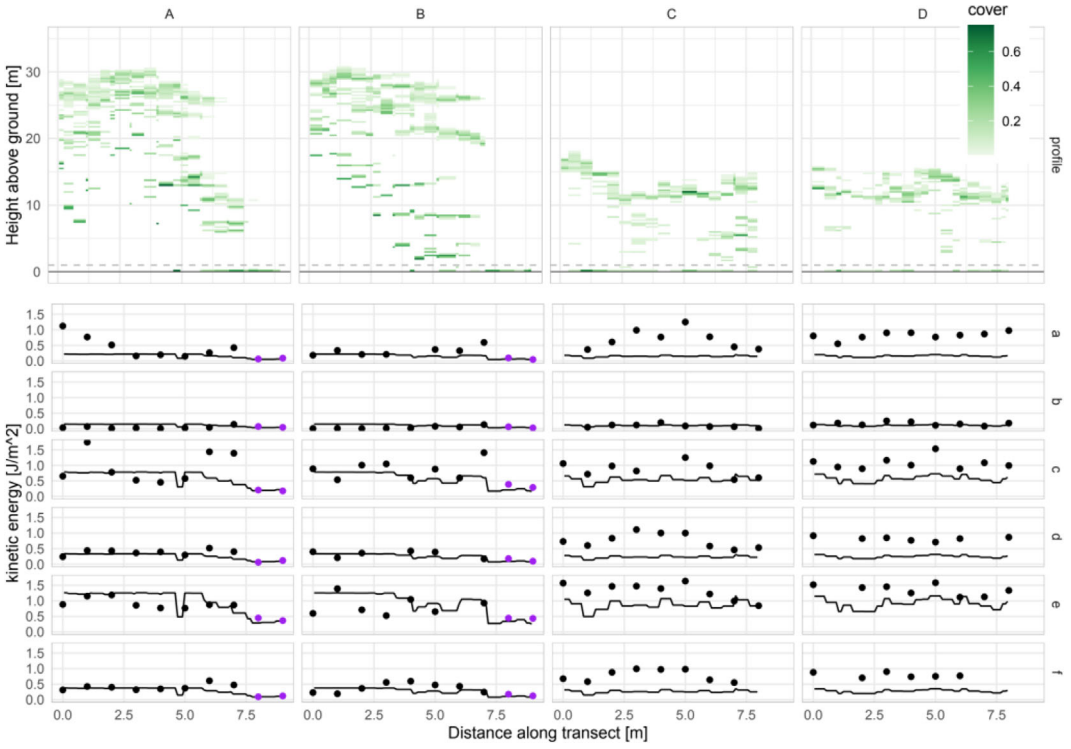

FIGURE 4 Transects through the vegetation cover voxel space (top). KE observations (black points: TKE, purple: FKE) and predictions (lines) of the individual timesteps (a–f).

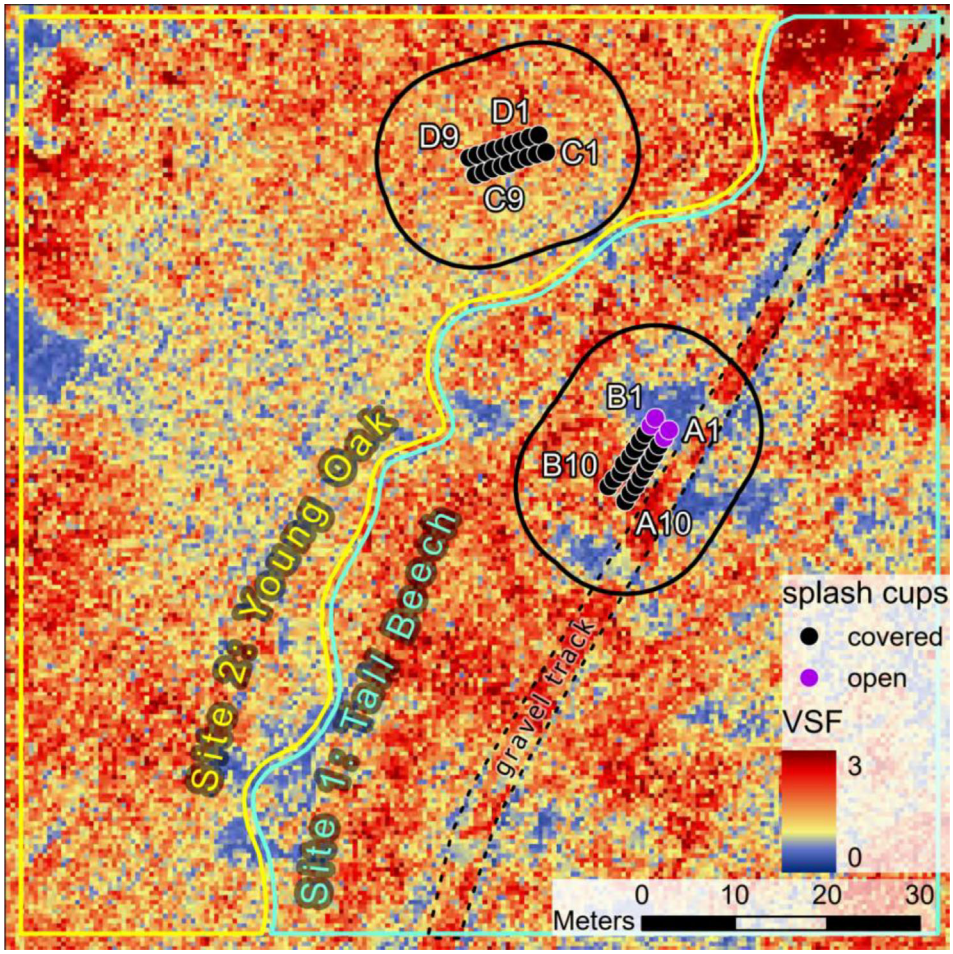

FIGURE 5 Map of the calculated VSF values, transects of splash cup positions with buffers for analysis, study sites and the gravel track.

TABLE 2 Statistical metrics of the VSF values calculated from the entire study area (combined area of the yellow and turquoise polygon in Figure 5) and the two buffered areas around the transects (black polygons in Figure 5).

	Study area	Buffer A + B	Buffer C + D
Min	0.27	0.28	0.42
Median	1.42	1.26	1.47
Mean	1.47	1.35	1.49
SD	0.60	0.68	0.47
Max	2.98	2.96	2.91

FIGURE 6 Histogram of the calculated VSF values for the buffers around the transects of the two sites. The buffer polygons can be found in Figure 5.

similarity; however, the histogram displays a contrasting distribution of values. The values on Site 2 resemble a normal distribution, while Site 1 exhibits a symmetrical peak below 1 and a second peak around 2. This finding coincides with the homogeneous or heterogeneous nature of the vegetation structures present at the respective sites.

We have extracted the values from the VSF raster at the cup locations. The mean VSF values at both sites were slightly lower than the average of the two buffered areas around the transects. We calculated VSF values around 0.5 at the open canopy positions (FKE positions) on Site 1. Furthermore, we have calculated the ratio between the KE measured at each cup and the mean of the four FKE cups for every timestep. We have then plotted the TKE/FKE ratios against the VSF to assess the correspondence of the predicted effect of vegetation on rainfall KE against the observed effect (Figure 7). We found significant but weak positive correlations for the timesteps **d, e** and **f** (at the 5% level), while **c** was not quite significant. Timestep **b** with extremely low precipitation volume was excluded from further analysis.

We calculated the mean TKE/FKE ratios over all timesteps (except **b**) for each cup to compensate for variations in precipitation characteristics between the events. Figure 8 shows a significant relationship between the predicted and observed effects.

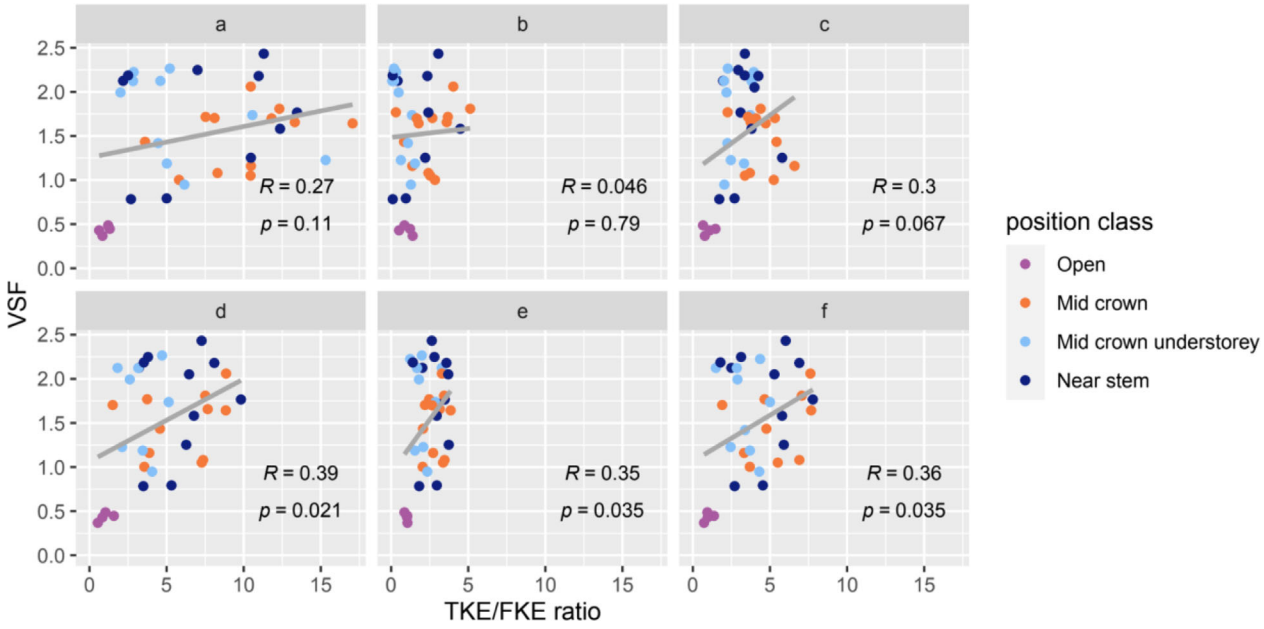

FIGURE 7 Scatterplots of the observed (TKE/FKE-ratio) and predicted (VSF) effect of vegetation on rainfall KE for all timesteps (facets) at each cup.

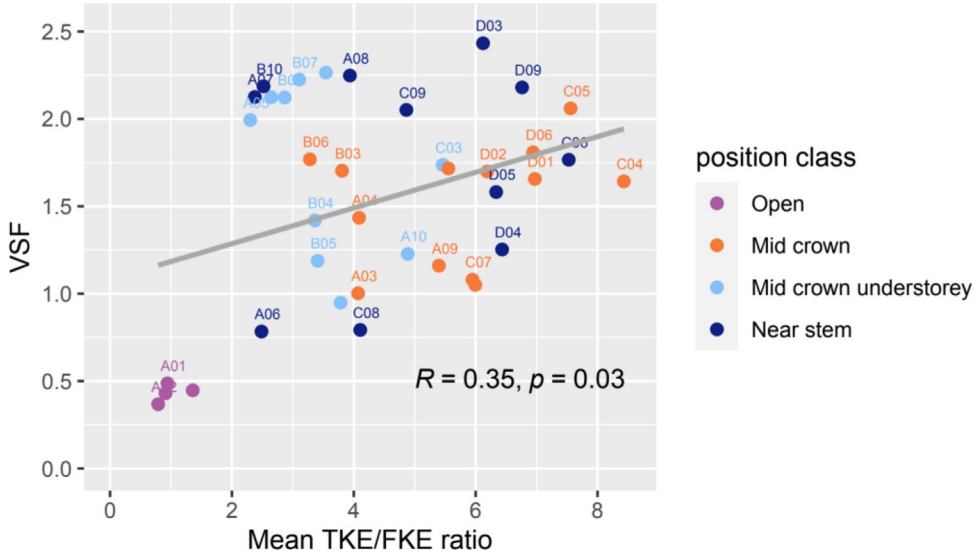

FIGURE 8 Scatterplot of the observed (TKE/FKE ratio) and predicted (VSF) effect of vegetation on rainfall KE averaged over all timesteps (except b) at each cup.

The value ranges of VSF and the TKE/FKE ratios deviate and have an overall RMSE of 3.43 (without **b**) with values of the timesteps varying between 1.27 (**e**) and 7.21 (**a**). This indicates that the model requires adaptation to the local ecosystem, which is in line with the suggestions made by Senn et al. (2020). To address this, we have tested whether the adaptation of the model can be improved by linearly scaling the VSF values. We calculated the smallest RMSE (2.08) when scaling the VSF by factor 2.66. As a result the mean VSF at the open positions increases from 0.43 to a more accurate 1.15.

3.2 | TKE prediction: Modelled erosivity of throughfall

We used the averaged FKE observations of each timestep to scale the calculated VSF values and thus estimate the resulting KE. These predictions are shown as black lines over the corresponding observations in Figure 4. We have also produced a scatterplot of the KE predictions and observations to visualise and assess the predictive ability of the model (Figure 9). Both Figures 4 and 9 suggest an overall underestimation of the predicted KE values. The underestimation of KE is more pronounced at Site 2. We calculated positive correlations (significant for **d**, **e**, **f** and trending in **c**) between TKE observations and predictions for all timesteps (except **b**) (Figure 9), which is analogous to Figure 7.

4 | DISCUSSION

The observed rainfall events were representative of the study area (DWD, 2024). While we found that overall FKE increased with precipitation, we observed large variations within the FKE measurements

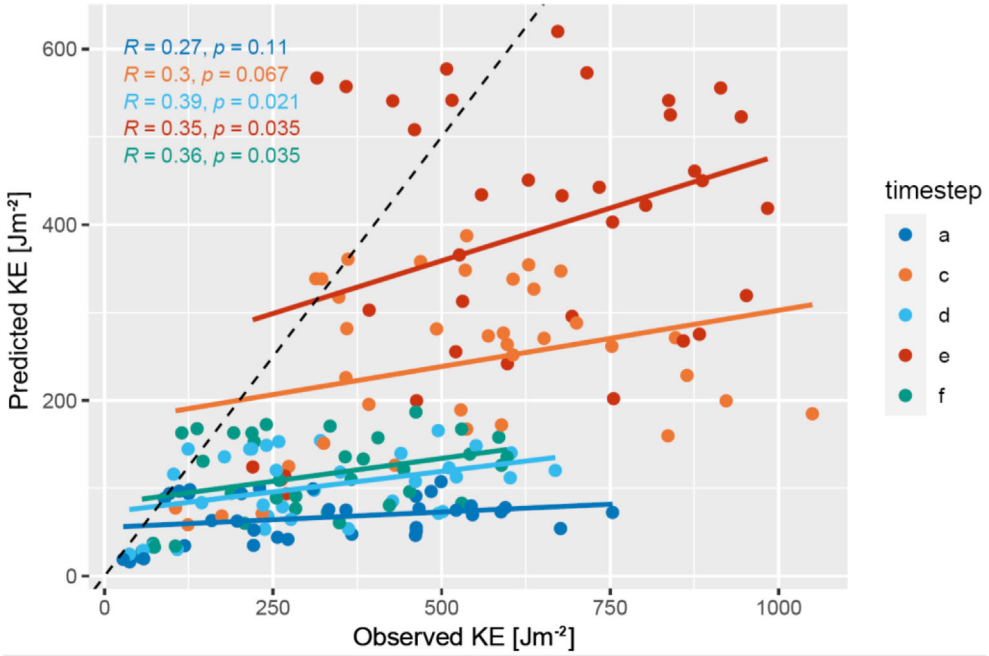

FIGURE 9 Scatterplot of the predicted and observed KE values at each cup, grouped by timestep.

normalised by rainfall amount (Table 1). This suggests that the characteristics of rainfall events are more determinant of KE than the amount of rainfall. In addition, the FKE measurements may have been affected by wind effects, because the survey design only included FKE measurements as part of the transects. Depending on the wind direction, the FKE measured in a small clearing might be susceptible to distortion of the DSD (Nanko et al., 2020; Nanko, Mizugaki, & Onda, 2008). The wind tends to interfere with raindrops at different extents depending on their size (known as winnowing). This alteration may have led to a decrease in the amount of rainfall and KE reaching the FKE cups in the open area. For future application, it is crucial to measure FKE well outside of the stand.

The measured TKE values differed significantly between the two sites and were twice as high at Site 2 (young oak) compared to Site 1 (tall beech). At Site 2, we found higher mean TKE values for each timestep and for the survey as a whole. These differences may be related to the higher canopy storage and retention capacity of the old growth beech stand at Site 1. Its higher complexity may have resulted in an increased likelihood of canopy drips being re-intercepted and dispersed into droplets before reaching the ground (Seitz et al., 2016). This effect of structural diversity is reflected in the TKE measurements, which at Site 1 vary greatly within the timesteps, while Site 2 showed smaller variation under the homogenous canopy of the young oaks.

The observed TKE/FKE ratios indicate a significant increase in KE caused by vegetation. We observed an average TKE/FKE ratio of 4.28, with means per event ranging between 1.71 and 8.01. This indicates that vegetation has at least doubled the KE of rainfall. The variation is especially large between the different rainfall events (Figure 7). These values are higher than those reported by previous studies who have reported ratios of 1.8 to 2.3 under rubber-based agroforestry systems (Liu et al., 2018), 1.8 and 2 under Japanese cypress plantations (Shinohara et al., 2018), 2.59 under tropical large leaved forests where TKE increased with successional stage (Geißler et al., 2012) and ratios close to 1 under young trees with an average height of 2.7 m (Goebes et al., 2015b). With regard to the first research question, our results showed higher TKE/FKE ratios than those reported in the literature. Contrary to our expectations, the results indicated a stronger vegetation effect under temperate forests compared to plantations exposed to tropical rain storms. Therefore, we consider that wind effects are a more plausible explanation for the systematic negative deviation of the FKE measurements.

In our case, the homogenous stand of lower oak trees with sparse understorey (Site 2) has resulted in higher TKE/FKE ratios compared to the taller and more heterogeneous beech stand (Site 1) featuring more but still sparse understorey. It is more meaningful to compare our findings with the existing literature for Site 2, given its plantation-like characteristics. However, there is a lack of studies focussing on TKE under natural heterogeneous forest structures, such as the beech stand at Site 1.

4.1 | VSF estimation

We have designed the VSF to reflect how vegetation affects the KE of rainfall analogously to the TKE/FKE ratio. In our KE measurements, we have observed differences in the magnitude and variation of KE that correspond to the three-dimensional structure of the forest stands. In the VSF map (Figure 5), Site 2 is characterised by small variations in values and gradual changes. These characteristics are reflected in a narrow histogram (Figure 6) and correspond to the uniformity of the vegetation structure in the young oak stand present at Site 2. The structurally diverse beech stand at Site 1 should lead to the opposite effect. Numerous openings in the canopy allow light to enter and encourage the growth of understorey. Vegetation parts are present at different heights. This structural pattern is reflected in the VSF map, where gaps in the canopy correspond to areas with lower VSF values, while tall trees with dense crowns are associated with high VSF values. As an example, the gravel track crossing Site 1 (shown as a dashed outline in Figure 5) is evidently an area without

an understorey but with a mostly closed canopy. This strip stands out because it has resulted in higher VSF values compared to its surroundings. However, the model returned low VSF values in a few places that coincide with gaps in the canopy. A similar VSF pattern along a gravel track has been reported by Senn et al. (2020).

The effect of this particular gravel track also underlines the general concept behind the VSF model, which can be understood particularly by the absence of understorey (Senn et al., 2020). This scenario of closed tree canopy without understorey represents the situation most prone to erosion by splash (highest VSF), whereas the scenario with understorey in direct neighbourhood represents the maximum contrast being the neutral case for erosion (VSF = 1). The good representation of these effects in the VSF map indicates the functioning of the VSF and the vegetation cover estimation from the ULS point cloud in the voxel space. We concluded that the spatial VSF patterns correspond to vegetation structure, thereby affirming the second research question.

To determine if the relationship between VSF and observed TKE/FKE properties extends beyond spatial patterns, we have created scatterplots (Figures 7 and 8). The scatterplots in Figure 7 show how the predicted effect of vegetation on TKE (VSF) corresponds to the observed effect (TKE/FKE ratio) for each cup. We found a significant statistical relationship that further highlights the potential of the VSF approach. Our results show that the predicted values correlate with the measurements. These findings confirm that a relationship exists between VSF and the TKE/FKE ratios, thereby addressing our third research question. The large variations between cups, position classes and timesteps are to be expected because of the effects of wind, rainfall variations and the limited size of the dataset.

The VSF model was developed based on observations from previous studies, which did not report TKE/FKE ratios higher than 3. However, in our study, we observed TKE/FKE ratios that exceed those previously reported, and as a result, the observed TKE/FKE ratios often exceeded the modelled VSF values. We believe that to parameterise a universally suitable VSF model, a larger dataset and more reliable FKE measurements are required.

The most noticeable deviations show under the canopies. At the open canopy positions, the TKE/FKE ratio was consistently 1 (neutral). However, the predicted VSF values were around 0.4 at the FKE positions, indicating a contradictory reduction relative to themselves. The reason for this discrepancy is that we defined the open canopy positions on the basis of the splash cup measurements. For the cup placement, we have defined open canopy positions as positions where there is no vegetation above the cups. However, it is important to note that vegetation is often not entirely absent; there (in the point cloud) may be ground-covering vegetation present beneath the splash cup. This was the case at the open canopy positions, resulting in VSF values below 1. The considerations of vertical cup placement lead to conflicts between two requirements: On the one hand, cups must be positioned at a certain height above the ground, to avoid the deposition of detached soil particles. Consequently, the KE measurements exclude the effect of any ground covering vegetation layers beneath. On the other hand, it is important to include the effect of the lowest layers in the model. We have accepted this divergence between observation and model. Future applications have to consider more closely how to avoid this issue. Ideally, KE would be measured at ground level, which is not feasible in a non-destructive way and without contamination by deposition. However, alternative approaches, such as using acoustic or piezoelectric signals to measure KE are still in their infancy.

The only truly unvegetated sections within the study area were the open canopy positions along the gravel track which was not suitable for splash cup placement. Here the VSF map indicates values close to 1.

We tested scaling the VSF as a simple approach for adapting the model to the observations. We found that the minimum overall RMSE between VSF and TKE/FKE ratio was achieved with a correction factor of 2.66. This also reduces the deviation of the VSF at the open positions by more than 70%.

4.2 | TKE prediction

Our second research question was to test if the VSF can be used to predict the TKE at the cup positions. The VSF is defined as the effect of vegetation on the KE of rainfall, that is, the TKE/FKE ratio. Accordingly, the TKE can be isolated by mathematical transformation. Thus, we predicted the TKE by linearly scaling the calculated VSF values with the FKE observations. Our approach is based on the assumption that initially the canopy storage is quickly filled up and afterwards the TKE increases linearly with the FKE. This initial threshold in rainfall volume was not reached by event **b** which we therefore excluded.

The results showed a significant correlation between the KE observations and the predicted values, indicating that the VSF can be used to predict rainfall erosivity answering question four. However, we found that the observed TKE values tended to exceed the predictions, especially at Site 2. This means the measured erosivity of rainfall under the canopies was higher than predicted. We assume this could have several reasons. Firstly, the VSF model was developed using a value range of 0 to 3, based on the TKE/FKE ratios reported in the literature. However, the TKE/FKE ratios observed in our study suggest that these rates of amplification may be too conservative. Secondly, the FKE measurements were taken from the open positions of the transects and not separately outside of the stand. Thus, the measurements may have underestimated FKE, for example, because of the winnowing effect. Such a systematic negative deviation of the FKE measurements would plausibly explain the systematic overestimation of the TKE/FKE ratios. Finally, the KE measurements with splash cups were performed above the ground covering vegetation and therefore missed out their protective effect.

The differences between the timesteps also suggest that the effect of vegetation on TKE was not linearly related to the FKE. This may be because of the retention effect of canopy storage (Nanko et al., 2020). Although the simple scaling of the VSF was suitable for demonstrating the feasibility of the approach in this study, the effect of canopy retention needs to be considered more in the future. A better representation of the retention effects requires better understanding of the processes involved. Therefore, future studies should incorporate additional measurements with higher temporal resolution. Variables such as rainfall volume, measured using tipping bucket rain gauges or DSD measured by laser disdrometers, can be employed to investigate canopy retention. The identified determinant vegetation traits could be derived from remote sensing data and incorporated in the model.

4.3 | Method evaluation

The significant correlation between the predicted and the observed TKE values confirms the general suitability of the proposed approach. Yet, the small scope of this experiment has resulted in strong variations in the TKE/FKE ratios between time steps and also between measurement positions. A better representation of the KE characteristics could be achieved by increasing the number of timesteps. This would allow for better coverage of the variations in rainfall intensities and phenological stages.

We assume that the large variations between events can be attributed to canopy storage and retention effects that differ depending on the temporal characteristics of rainfall events. Adding tipping rain gauges at selected freefall and canopy positions would be valuable for investigating the effects of the temporal distribution of rainfall intensities. We believe that a good share of the unexplained variation can be attributed to storage effects. Therefore, we suggest developing a continuous gash-style interception model that can be parameterised using canopy storage potential derived from the same lidar dataset utilised by the VSF model (Gash, 1979; Muzylo et al., 2009).

Besides increasing the temporal coverage, it is even more important to increase the spatial coverage, that is, the sample size. We used a transect-based design to simplify spatial attribution. However, this approach resulted in cup positions that tended to represent the extremes of vegetation cover, specifically closed tall canopy or open positions. Consequently, there was a lack of intermediate vegetation cover configurations. When we excluded either the open or canopy measurement positions, the data showed no significant correlation. To address this, future studies should prioritise stratification across the entire gradient to capture a more complete range of throughfall variations. Additionally, open canopy positions should be located even more rigorously outside the stand. A larger number of splash cup measurements will improve the significance of the dataset (Goebes et al., 2015b, 2016; Liu et al., 2018). Previous studies have highlighted the need for more comprehensive datasets on erosivity covering the variation of TKE and its drivers that include species, trait expression, ecosystems and vegetation zones (Fernández-Raga et al., 2013; Geißler et al., 2013; Goebes et al., 2016; Levia et al., 2019; Nanko et al., 2020). Combining KE data from more diverse stands with aerial lidar can improve our understanding of the processes and help to optimise the VSF model. Eventually less in situ data will be required in order to predict TKE over larger areas.

The parametrisation of the model (height-dependent weighting factor) is currently based on stochastic findings from the literature. Eventually, this parametrisation could be based on the physical relationships between DSD, falling heights and the resulting impact velocities (Kattge et al., 2020).

One of the most influential variables in the calculation of the VSF is the gap fraction voxel dataset. For model performance, it is crucial that the data closely represent the actual vegetation cover gaps. Literature indicates that the calculated gap fraction and its derivative LAD are highly dependent on the applied voxel size (Ross et al., 2022) and the scan angle filtering (Almeida et al., 2019). The VSF model simplistically assumes an even distribution of vegetation surfaces per voxel and predicts the probability of throughfall according to the corresponding gap fraction. However, in reality, vegetation surfaces are often spatially clustered. Consequently, the smaller the cells, the better the spatial representation and vertical attribution of vegetation surfaces. The applied gap fraction calculation approach (Bouvier et al., 2015) is based on the assumption that every surface present can be reached by the laser pulse. However, in reality there are occluded voxels that no pulse ever reaches (Kükenbrink et al., 2017). This is especially an issue in sparser ALS point clouds but even with high point densities of ULS point clouds, and a high percentage of areas below the canopy may remain occluded (Kükenbrink et al., 2017; Schneider et al., 2019).

ULS and ALS can furthermore differ in the scan geometry, namely flying height, view angle and line spacing. Including multiple view angles can be favourable to minimise or detect occluded voxels (Yin, Cook, & Morton, 2022). This is because canopy gaps allow diagonal beams to penetrate more easily sideways into a voxel. However, off-nadir beam angles travel further through the canopy and are thus more likely to be obscured and not deliver returns from lower canopy parts (Liu, Liu, & Zhu, 2018). The angle dependence differs between tree species, where coniferous trees are more affected than deciduous trees (horizontal leaf orientation) (Liu, Liu, & Zhu, 2018). While not possible in the framework of this study, it would be sensible to collect ground truth data as a reference for the gap fraction. Suitable reference data can either be acquired by visual estimation, hemispherical photographs or using ground-based lidar (Almeida et al., 2019).

We found that using returns from all scan angles without filtering led to better correspondence between the VSF and the TKE/FKE ratio. Our ULS dataset was captured from a flying height below 80 m and consequently features a narrow line spacing and a large range of scan angles. Only a limited number of returns clustered along the flight lines come from near-nadir scan angles and are thus spatially unevenly distributed. We assume that filtering our ULS dataset by the scan angle would have removed too many returns. Avoiding occluded pixels was more impactful than sticking to the vertical scan geometry. This agrees with the findings of Liu, Liu and Zhu (2018), who found that gap fraction accuracy under deciduous stands is not affected by inclusion of oblique scan angles. Future studies should consider scan geometry and vegetation characteristics in ULS and ALS surveys.

5 | CONCLUSIONS

This work aimed to test the VSF model that was designed to predict the effect of vegetation on rainfall erosivity over larger areas using aerial lidar point clouds. In the framework of this study, we have successfully demonstrated that TKE can be predicted from remotely sensed forest vegetation structures.

We have proved that VSF maps spatially continuously represent the effect of vegetation on the KE of rainfall on a small tree stand scale. In particular, the model reproduces both the amplifying and the reducing properties, making it a promising addition to erosion modelling approaches. Furthermore, VSF maps can be scaled by in situ FKE measurements to spatially continuously predict the KE and thus the erosivity of rainfall reaching the ground. The method can provide good indications, but further tests and improvements are required for precise predictions. The VSF model is therefore suitable to extend the methodological tool box in erosion studies under vegetation and to support decision-makers in forestry and also agriculture.

We intentionally kept the model simple by incorporating only the three-dimensional distribution of vegetation surfaces, yet it yielded significant results. The VSF model was parameterised based on TKE/FKE ratios reported in previous literature; however, the TKE/FKE ratios observed in our study exceeded those reported in the literature. This is most likely because of the placement of the FKE measurements. Consequently, the observed TKE values systematically exceed those predicted using the VSF. To improve the model for future applications, the model should be optimised using additional data and experience from more measurement campaigns in other ecosystems. Such studies should also investigate for which spatial and temporal scales the VSF is applicable.

Future model implementations should improve the calibration of the weighting factor and adapt the model to individual plant species. Moreover, they could also consider calculating the VSF based directly on physical laws (e.g. falling height, DSD, acceleration rates) instead of relying on stochastic relationships. Another promising measure to improve the model would be to include metrics of canopy storage and retention, which are particularly determinant in less abundant precipitation events. The VSF has proved suitable solely relying on structural traits. We appreciate that there are many other influential traits. For potentially incorporating additional plant parameters (e.g. tree and leaf traits), it is valuable that previous studies have identified the relevant traits.

The simplicity of the current model makes it easy to apply, and the code is published on github. Therefore, we are confident that the VSF model can be adopted widely by other researchers to investigate rainfall erosivity in other ecosystems and to test the approach on larger scales. Another application pathway would be adapting the model to the GEDI satellite-based lidar product to calculate the VSF for larger areas. The VSF model has proven reliable, and one promising application could be the representation of vegetation in large erosion models such as USLE. Using the VSF for the crop factor would strongly improve the level of detail in which vegetation is represented.

Despite the presented limitations, this pilot study yields several important merits: Firstly, we have demonstrated the general suitability of the VSF model; secondly, we have presented and tested a spatially continuous approach for an issue previously limited to plots; thirdly, we have observed discrepancies between the literature and our observations for rainfall KE under temperate forests; and finally, we have identified limitations of the approach and presented specific strategies for improving.

ACKNOWLEDGEMENTS

We would like to thank Hannah Weiser for her patient support with the point cloud pre-processing and Sabine Flaiz for her support with the lab work. Furthermore, we would like to thank Fabian Fassnacht for his support. Open Access funding enabled and organized by Projekt DEAL.

CONFLICT OF INTEREST STATEMENT

The authors declare no conflict of interest.

DATA AVAILABILITY STATEMENT

The data that support the findings of this study are available from the corresponding author upon reasonable request.

ORCID

Johannes Antenor Senn https://orcid.org/0000-0001-6627-2568

REFERENCES

Abe, H., Kume, T., Hyodo, F., Oyamada, M. & Katayama, A. (2024) Soil erosion under forest hampers beech growth: impacts of understory vegetation degradation by sika deer. *Catena*, 234, 107559. Available from: https://doi.org/10.1016/j.catena.2023.107559

Åkerblom, M. & Kaitaniemi, P. (2021) Terrestrial laser scanning: a new standard of forest measuring and modelling? *Annals of Botany*, 128(6), 653–662. Available from: https://doi.org/10.1093/aob/mcab111

Alivio, M.B., Bezak, N. & Mikoš, M. (2023) The size distribution metrics and kinetic energy of raindrops above and below an isolated tree canopy in urban environment. *Urban Forestry & Urban Greening*, 85, 127971. Available from: https://doi.org/10.1016/j.ufug.2023.127971

Almeida, D.R.A.D., Stark, S.C., Shao, G., Schietti, J., Nelson, B.W., Silva, C.A., et al. (2019) Optimizing the remote detection of tropical rainforest structure with airborne lidar: leaf area profile sensitivity to pulse density and spatial sampling. *Remote Sensing*, 11(1), 92. Available from: https://doi.org/10.3390/rs11010092

Angulo-Martínez, M., Beguería, S., Latorre, B. & Fernández-Raga, M. (2018) Comparison of precipitation measurements by OTT Parsivel2 and Thies LPM optical disdrometers. *Hydrology and Earth System Sciences*, 22(5), 2811–2837. Available from: https://doi.org/10.5194/hess-22-2811-2018

Beniaich, A., Silva, M.L.N., Guimarães, D.V., Avalos, F.A.P., Terra, F.S., Menezes, M.D., et al. (2022) UAV-based vegetation monitoring for assessing the impact of soil loss in olive orchards in Brazil. *Geoderma Regional*, 30, e00543. Available from: https://doi.org/10.1016/j.geodrs.2022.e00543

Bouvier, M., Durrieu, S., Fournier, R.A. & Renaud, J.-P. (2015) Generalizing predictive models of forest inventory attributes using an area-based approach with airborne LiDAR data. *Remote Sensing of Environment*, 156, 322–334. Available from: https://doi.org/10.1016/j.rse.2014.10.004

Boyd, D.S. & Foody, G.M. (2011) An overview of recent remote sensing and GIS based research in ecological informatics. *Ecological Informatics*, 6(1), 25–36. Available from: https://doi.org/10.1016/j.ecoinf.2010.07.007

Calder, I.R. (1996) Dependence of rainfall interception on drop size: 1. Development of the two-layer stochastic model. *Journal of Hydrology*, 185(1–4), 1–4. Available from: https://doi.org/10.1016/0022-1694(95)02998-2

Calder, I.R. (2001) Canopy processes: implications for transpiration, interception and splash induced erosion, ultimately for forest management and water resources. In: Linsenmair, K.E., Davis, A.J., Fiala, B. & Speight, M.R. (Eds.) *Tropical forest canopies: ecology and management*, Vol. 69. Dodrecht, NL: Springer, pp. 203–214. https://doi.org/10.1007/978-94-017-3606-0

Chapman, G. (1948) Size of raindrops and their striking force at the soil surface in a red pine plantation. *Eos, Transactions American Geophysical Union*, 29(5), 664–670. Available from: https://doi.org/10.1029/TR029i005p00664

Cherif, E., Feilhauer, H., Berger, K., Dao, P.D., Ewald, M., Hank, T.B., et al. (2023) From spectra to plant functional traits: transferable multi-trait models from heterogeneous and sparse data. *Remote Sensing of Environment*, 292, 113580. Available from: https://doi.org/10.1016/j.rse.2023.113580

Dunkerley, D. (2020) A review of the effects of throughfall and stemflow on soil properties and soil erosion. In: Van Stan, J.T., II, Gutmann, E. & Friesen, J. (Eds.) *Precipitation partitioning by vegetation*. Cham, CH: Springer International Publishing, pp. 183–214. https://doi.org/10.1007/978-3-030-29702-2_12

DWD. (2024) Tägliche Niederschlagsbeobachtungen für Deutschland RR_00710 (No. urn:wmo:md:de-dwd-cdc:obsgermany-climate-daily-more_precip; Version v24.3) [Dataset]. Climate Data Center (CDC).

https://opendata.dwd.de/climate_environment/CDC/observations_germany/climate/daily/more_precip/historical/

Ellison, W.D. (1948a) Erosion by raindrop. *Scientific American*, 179(5), 40–45. Available from: https://doi.org/10.1038/scientificamerican1148-40

Ellison, W.D. (1948b) Soil erosion. *Soil Science Society of America Journal*, 12(C), 479–484. Available from: https://doi.org/10.2136/sssaj1948.036159950012000C0107x

Exler, J.L. & Moore, R.D. (2022) Quantifying throughfall, stemflow and interception loss in five vegetation communities in a maritime raised bog. *Agricultural and Forest Meteorology*, 327, 109202. Available from: https://doi.org/10.1016/j.agrformet.2022.109202

Fernández-Raga, M., Campo, J., Rodrigo-Comino, J. & Keesstra, S.D. (2019) Comparative analysis of splash erosion devices for rainfall simulation experiments: a laboratory study. *Water*, 11(6), 1228. Available from: https://doi.org/10.3390/w11061228

Fernández-Raga, M., Marques, R.L.C., Varela, M.E., Martins, M.A.S., Porras, E.M., Fraile, R. & Keizer, J.J. (2013) *Splash erosion in recently-burnt terraced eucalypt plantations in north-central Portugal*. https://sites.google.com/site/flammafgr/texto/volumen-4-2013/4-2-2013/4_2_7/4_2_7.pdf

Fernández-Raga, M., Palencia, C., Keesstra, S., Jordán, A., Fraile, R., Angulo-Martínez, M., et al. (2017) Splash erosion: a review with unanswered questions. *Earth-Science Reviews*, 171, 463–477. Available from: https://doi.org/10.1016/j.earscirev.2017.06.009

Foot, K. & Morgan, R.P.C. (2005) The role of leaf inclination, leaf orientation and plant canopy architecture in soil particle detachment by raindrops. *Earth Surface Processes and Landforms*, 30(12), 1509–1520. Available from: https://doi.org/10.1002/esp.1207

Gall, C., Nebel, M., Quandt, D., Scholten, T. & Seitz, S. (2022) Pioneer biocrust communities prevent soil erosion in temperate forests after disturbances. *Biogeosciences*, 19(13), 3225–3245. Available from: https://doi.org/10.5194/bg-19-3225-2022

Gash, J.H.C. (1979) An analytical model of rainfall interception by forests. *Quarterly Journal of the Royal Meteorological Society*, 105(443), 43–55. Available from: https://doi.org/10.1002/qj.49710544304

Geißler, C., Kühn, P., Böhnke, M., Bruelheide, H., Shi, X. & Scholten, T. (2012) Splash erosion potential under tree canopies in subtropical SE China. *Catena*, 91, 85–93. Available from: https://doi.org/10.1016/j.catena.2010.10.009

Geißler, C., Nadrowski, K., Kühn, P., Baruffol, M., Bruelheide, H., Schmid, B., et al. (2013) Kinetic energy of throughfall in subtropical forests of SE China—effects of tree canopy structure, functional traits, and biodiversity. *PLoS ONE*, 8(2), 2. Available from: https://doi.org/10.1371/journal.pone.0049618

Ghadiri, H. & Payne, D. (1981) Raindrop impact stress. *Journal of Soil Science*, 32(1), 41–49. Available from: https://doi.org/10.1111/j.1365-2389.1981.tb01684.x

Ghadiri, H. & Payne, D. (1986) The risk of leaving the soil surface unprotected against falling rain. *Soil and Tillage Research*, 8, 119–130. Available from: https://doi.org/10.1016/0167-1987(86)90328-4

Goebes, P., Schmidt, K., Härdtle, W., Seitz, S., Stumpf, F., von Oheimb, G., et al. (2016) Rule-based analysis of throughfall kinetic energy to evaluate biotic and abiotic factor thresholds to mitigate erosive power. *Progress in Physical Geography*, 40(3), 3. Available from: https://doi.org/10.1177/0309133315624642

Goebes, P., Seitz, S., Geißler, C., Lassu, T., Peters, P., Seeger, M., et al. (2014) Momentum or kinetic energy? How do substrate properties influence the calculation of rainfall erosivity? *Journal of Hydrology*, 517, 310–316. Available from: https://doi.org/10.1016/j.jhydrol.2014.05.031

Goebes, P., Seitz, S., Kühn, P., Kröber, W., Bruelheide, H., Li, Y., von Oheimb, G. & Scholten, T. (2015a) Species-specific effects on throughfall kinetic energy below 12 subtropical tree species are related to leaf traits and tree architecture. EGU General Assembly Conference Abstracts, 17, 3942. http://adsabs.harvard.edu/abs/2015EGUGA..17.3942G

Goebes, P., Seitz, S., Kühn, P., Li, Y., Niklaus, P.A., von Oheimb, G., et al. (2015b) Throughfall kinetic energy in young subtropical forests: investigation on tree species richness effects and spatial variability. *Agricultural and Forest Meteorology*, 213, 148–159. Available from: https://doi.org/10.1016/j.agrformet.2015.06.019

Gonsamo, A., D'odorico, P. & Pellikka, P. (2013) Measuring fractional forest canopy element cover and openness—definitions and methodologies revisited. *Oikos*, 122(9), 9. Available from: https://doi.org/10.1111/j.1600-0706.2013.00369.x

Gunn, R. & Kinzer, G.D. (1949) The terminal velocity of fall for water droplets in stagnant air. *Journal of Atmospheric Sciences*, 6(4), 243–248.

Herwitz, S.R. (1987) Raindrop impact and water flow on the vegetative surfaces of trees and the effects on stemflow and throughfall generation. *Earth Surface Processes and Landforms*, 12(4), 4. Available from: https://doi.org/10.1002/esp.3290120408

Hyyppä, E., Hyyppä, J., Hakala, T., Kukko, A., Wulder, M.A., White, J.C., et al. (2020) Under-canopy UAV laser scanning for accurate forest field measurements. *ISPRS Journal of Photogrammetry and Remote Sensing*, 164, 41–60. Available from: https://doi.org/10.1016/j.isprsjprs.2020.03.021

Itakura, K. & Hosoi, F. (2019) Estimation of leaf inclination angle in three-dimensional plant images obtained from lidar. *Remote Sensing*, 11(3), 344. Available from: https://doi.org/10.3390/rs11030344

Ji, S., Omar, S.I., Zhang, S., Wang, T., Chen, C. & Zhang, W. (2022) Comprehensive evaluation of throughfall erosion in the banana plantation. *Earth Surface Processes and Landforms*, 47(12), 2941–2949. Available from: https://doi.org/10.1002/esp.5435

Johannsen, L.L., Zambon, N., Strauss, P., Dostal, T., Neumann, M., Zumr, D., et al. (2020) Comparison of three types of laser optical disdrometers under natural rainfall conditions. *Hydrological Sciences Journal*, 65(4), 524–535. Available from: https://doi.org/10.1080/02626667.2019.1709641

Katayama, A., Nanko, K., Jeong, S., Kume, T., Shinohara, Y. & Seitz, S. (2023) Short communication: concentrated impacts by tree canopy drips—hotspots of soil erosion in forests. *Earth Surface Dynamics*, 11(6), 1275–1282. Available from: https://doi.org/10.5194/esurf-11-1275-2023

Kattenborn, T., Fassnacht, F.E. & Schmidtlein, S. (2019) Differentiating plant functional types using reflectance: which traits make the difference? *Remote Sensing in Ecology and Conservation*, 5(1), 5–19. Available from: https://doi.org/10.1002/rse2.86

Kattenborn, T., Richter, R., Guimarães-Steinicke, C., Feilhauer, H. & Wirth, C. (2022) Anglecam: predicting the temporal variation of leaf angle distributions from image series with deep learning. *Methods in Ecology and Evolution*, 13(11), 2531–2545. Available from: https://doi.org/10.1111/2041-210X.13968

Kattge, J., Bönisch, G., Díaz, S., Lavorel, S., Prentice, I.C., Leadley, P., et al. (2020) TRY plant trait database—enhanced coverage and open access. *Global Change Biology*, 26(1), 119–188. Available from: https://doi.org/10.1111/gcb.14904

Kükenbrink, D., Schneider, F.D., Leiterer, R., Schaepman, M.E. & Morsdorf, F. (2017) Quantification of hidden canopy volume of airborne laser scanning data using a voxel traversal algorithm. *Remote Sensing of Environment*, 194, 424–436. Available from: https://doi.org/10.1016/j.rse.2016.10.023

Lacombe, G., Valentin, C., Sounyafong, P., de Rouw, A., Soulileuth, B., Silvera, N., et al. (2018) Linking crop structure, throughfall, soil surface conditions, runoff and soil detachment: 10 land uses analyzed in Northern Laos. *Science of the Total Environment*, 616, 1330–1338. Available from: https://doi.org/10.1016/j.scitotenv.2017.10.185

Lechner, A.M., Foody, G.M. & Boyd, D.S. (2020) Applications in remote sensing to forest ecology and management. *One Earth*, 2(5), 405–412. Available from: https://doi.org/10.1016/j.oneear.2020.05.001

Levia, D.F., Hudson, S.A., Llorens, P. & Nanko, K. (2017) Throughfall drop size distributions: a review and prospectus for future research: Throughfall drop size distributions. *Wiley Interdisciplinary Reviews: Water*, 4, e1225. Available from: https://doi.org/10.1002/wat2.1225

Levia, D.F., Nanko, K., Amasaki, H., Giambelluca, T.W., Hotta, N., Iida, S., et al. (2019) Throughfall partitioning by trees. *Hydrological Processes*, 33(12), 1698–1708. Available from: https://doi.org/10.1002/hyp.13432

Liu, J., Liu, W. & Zhu, K. (2018) Throughfall kinetic energy and its spatial characteristics under rubber-based agroforestry systems. *Catena*,

161, 113–121. Available from: https://doi.org/10.1016/j.catena.2017.10.014

Liu, J., Skidmore, A.K., Jones, S., Wang, T., Heurich, M., Zhu, X., et al. (2018) Large off-nadir scan angle of airborne LiDAR can severely affect the estimates of forest structure metrics. *ISPRS Journal of Photogrammetry and Remote Sensing*, 136, 13–25. Available from: https://doi.org/10.1016/j.isprsjprs.2017.12.004

Liu, J., Skidmore, A.K., Wang, T., Zhu, X., Premier, J., Heurich, M., et al. (2019) Variation of leaf angle distribution quantified by terrestrial LiDAR in natural European beech forest. *ISPRS Journal of Photogrammetry and Remote Sensing*, 148, 208–220. Available from: https://doi.org/10.1016/j.isprsjprs.2019.01.005

Liu, W., Luo, Q., Lu, H., Wu, J. & Duan, W. (2017) The effect of litter layer on controlling surface runoff and erosion in rubber plantations on tropical mountain slopes, SW China. *Catena*, 149, 167–175. Available from: https://doi.org/10.1016/j.catena.2016.09.013

Ma, B., Liu, Y., Liu, X., Ma, F., Wu, F. & Li, Z. (2015) Soil splash detachment and its spatial distribution under corn and soybean cover. *Catena*, 127, 142–151. Available from: https://doi.org/10.1016/j.catena.2014.11.009

Marzen, M. & Iserloh, T. (2021) Processes of raindrop splash and effects on soil erosion. In: *Precipitation*. London, UK: Elsevier, pp. 351–371. https://doi.org/10.1016/B978-0-12-822699-5.00013-6

Miura, S., Ugawa, S., Yoshinaga, S. & Keizo Hirai, T.Y. (2015) Floor cover percentage determines splash erosion in *Chamaecyparis obtusa* forests. *Soil Science Society of America Journal*, 79(6), 1782–1791. Available from: https://doi.org/10.2136/sssaj2015.05.0171

Morgan, R.P.C. (2005) *Soil erosion and conservation*, 3rd edition. Oxford, UK: Blackwell Pub.

Morsdorf, F., Kötz, B., Meier, E., Itten, K.I. & Allgöwer, B. (2006) Estimation of LAI and fractional cover from small footprint airborne laser scanning data based on gap fraction. *Remote Sensing of Environment*, 104(1), Article 1. Available from: https://doi.org/10.1016/j.rse.2006.04.019

Muzylo, A., Llorens, P., Valente, F., Keizer, J.J., Domingo, F. & Gash, J.H.C. (2009) A review of rainfall interception modelling. *Journal of Hydrology*, 370(1–4), 191–206. Available from: https://doi.org/10.1016/j.jhydrol.2009.02.058

Nanko, K., Hotta, N. & Suzuki, M. (2004) Assessing raindrop impact energy at the forest floor in a mature Japanese cypress plantation using continuous raindrop-sizing instruments. *Journal of Forest Research*, 9(2), 2. Available from: https://doi.org/10.1007/s10310-003-0067-6

Nanko, K., Hotta, N. & Suzuki, M. (2006) Evaluating the influence of canopy species and meteorological factors on throughfall drop size distribution. *Journal of Hydrology*, 329(3–4), Article 3–4. Available from: https://doi.org/10.1016/j.jhydrol.2006.02.036

Nanko, K., Hudson, S.A. & Levia, D.F. (2016) Differences in throughfall drop size distributions in the presence and absence of foliage. *Hydrological Sciences Journal*, 61(3), 3. Available from: https://doi.org/10.1080/02626667.2015.1052454

Nanko, K., Mizugaki, S. & Onda, Y. (2008) Estimation of soil splash detachment rates on the forest floor of an unmanaged Japanese cypress plantation based on field measurements of throughfall drop sizes and velocities. *Catena*, 72(3), 3. Available from: https://doi.org/10.1016/j.catena.2007.07.002

Nanko, K., Onda, Y., Ito, A. & Moriwaki, H. (2008) Effect of canopy thickness and canopy saturation on the amount and kinetic energy of throughfall: an experimental approach. *Geophysical Research Letters*, 35(5), 5. Available from: https://doi.org/10.1029/2007GL033010

Nanko, K., Tanaka, N., Leuchner, M. & Levia, D.F. (2020) Throughfall erosivity in relation to drop size and crown position: a case study from a teak plantation in Thailand. In: Levia, D.F., Carlyle-Moses, D.E., Iida, S., Michalzik, B., Nanko, K. & Tischer, A. (Eds.) *Forest-water interactions*, Vol. 240. Cham, CH: Springer International Publishing, pp. 279–298. https://doi.org/10.1007/978-3-030-26086-6_12

Panagos, P., Borrelli, P., Meusburger, K., Alewell, C., Lugato, E. & Montanarella, L. (2015) Estimating the soil erosion cover-management factor at the European scale. *Land Use Policy*, 48, 38–50. Available from: https://doi.org/10.1016/j.landusepol.2015.05.021

Ross, C.W., Loudermilk, E.L., Skowronski, N., Pokswinski, S., Hiers, J.K. & O'Brien, J. (2022) LiDAR voxel-size optimization for canopy gap estimation. *Remote Sensing*, 14(5), 1054. Available from: https://doi.org/10.3390/rs14051054

Roussel, J.-R. & Auty, D. (2024) Airborne LiDAR data manipulation and visualization for forestry applications. https://cran.r-project.org/package=lidR

Roussel, J.-R., Auty, D., Coops, N.C., Tompalski, P., Goodbody, T.R.H., Meador, A.S., et al. (2020) lidR: An R package for analysis of airborne laser scanning (ALS) data. *Remote Sensing of Environment*, 251, 112061. Available from: https://doi.org/10.1016/j.rse.2020.112061

Schneider, F.D., Kükenbrink, D., Schaepman, M.E., Schimel, D.S. & Morsdorf, F. (2019) Quantifying 3d structure and occlusion in dense tropical and temperate forests using close-range LiDAR. *Agricultural and Forest Meteorology*, 268, 249–257. Available from: https://doi.org/10.1016/j.agrformet.2019.01.033

Scholten, T., Geißler, C., Goc, J., Kühn, P. & Wiegand, C. (2011) A new splash cup to measure the kinetic energy of rainfall. *Journal of Plant Nutrition and Soil Science*, 174(4), 596–601. Available from: https://doi.org/10.1002/jpln.201000349

Scholten, T. & Seitz, S. (2019) Soil erosion and land degradation. *Soil Systems*, 3(4), 68. Available from: https://doi.org/10.3390/soilsystems3040068

Schumacher, J. & Christiansen, J.R. (2020) LiDAR applications to forest-water interactions. In: Levia, D.F., Carlyle-Moses, D.E., Iida, S., Michalzik, B., Nanko, K. & Tischer, A. (Eds.) *Forest-water interactions*, Vol. 240. Cham, CH: Springer International Publishing, pp. 87–112. https://doi.org/10.1007/978-3-030-26086-6_4

Seitz, S., Goebes, P., Song, Z., Bruelheide, H., Härdtle, W., Kühn, P., et al. (2016) Tree species and functional traits but not species richness affect interrill erosion processes in young subtropical forests. *The Soil*, 2(1), 49–61. Available from: https://doi.org/10.5194/soil-2-49-2016

Seitz, S., Nebel, M., Goebes, P., Käppeler, K., Schmidt, K., Shi, X., et al. (2017) Bryophyte-dominated biological soil crusts mitigate soil erosion in an early successional Chinese subtropical forest. *Biogeosciences*, 14(24), 5775–5788. Available from: https://doi.org/10.5194/bg-14-5775-2017

Senn, J.A., Fassnacht, F.E., Eichel, J., Seitz, S. & Schmidtlein, S. (2020) A new concept for estimating the influence of vegetation on throughfall kinetic energy using aerial laser scanning. *Earth Surface Processes and Landforms*, 45(7), esp.4820. Available from: https://doi.org/10.1002/esp.4820

Sepuru, T.K. & Dube, T. (2018) An appraisal on the progress of remote sensing applications in soil erosion mapping and monitoring. *Remote Sensing Applications: Society and Environment*, 9, 1–9.

Serio, M.A., Carollo, F.G. & Ferro, V. (2019) Raindrop size distribution and terminal velocity for rainfall erosivity studies. A review. *Journal of Hydrology*, 576, 210–228. Available from: https://doi.org/10.1016/j.jhydrol.2019.06.040

Shinohara, Y., Ichinose, K., Morimoto, M., Kubota, T. & Nanko, K. (2018) Factors influencing the erosivity indices of raindrops in Japanese cypress plantations. *Catena*, 171, 54–61. Available from: https://doi.org/10.1016/j.catena.2018.06.030

Song, Z., Seitz, S., Zhu, P., Goebes, P., Shi, X., Xu, S., et al. (2018) Spatial distribution of LAI and its relationship with throughfall kinetic energy of common tree species in a Chinese subtropical forest plantation. *Forest Ecology and Management*, 425, 189–195. Available from: https://doi.org/10.1016/j.foreco.2018.05.046

Van Dijk, A.I.J.M., Meesters, A.G.C.A. & Bruijnzeel, L.A. (2002) Exponential distribution theory and the interpretation of splash detachment and transport experiments. *Soil Science Society of America Journal*, 66(5), 1466–1474. Available from: https://doi.org/10.2136/sssaj2002.1466

Vrieling, A. (2006) Satellite remote sensing for water erosion assessment: a review. *Catena*, 65(1), 2–18. Available from: https://doi.org/10.1016/j.catena.2005.10.005

Weiser, H., Winiwarter, L., Anders, K., Fassnacht, F.E. & Höfle, B. (2021) Opaque voxel-based tree models for virtual laser scanning in forestry

applications. *Remote Sensing of Environment*, 265, 112641. Available from: https://doi.org/10.1016/j.rse.2021.112641

Xu, H., Hu, X., Guan, H., Zhang, B., Wang, M., Chen, S., et al. (2019) A remote sensing based method to detect soil erosion in forests. *Remote Sensing*, 11(5), 513. Available from: https://doi.org/10.3390/rs11050513

Yin, T., Cook, B.D. & Morton, D.C. (2022) Three-dimensional estimation of deciduous forest canopy structure and leaf area using multi-directional, leaf-on and leaf-off airborne lidar data. *Agricultural and Forest Meteorology*, 314, 108781. Available from: https://doi.org/10.1016/j.agrformet.2021.108781

Zemke, J. (2016) Runoff and soil erosion assessment on forest roads using a small scale rainfall simulator. *Hydrology*, 3(3), 25. Available from: https://doi.org/10.3390/hydrology3030025

Zhang, H., Yu, D., Dong, L., Shi, X., Warner, E., Gu, Z., et al. (2014) Regional soil erosion assessment from remote sensing data in rehabilitated high density canopy forests of southern China. *Catena*, 123, 106–112. Available from: https://doi.org/10.1016/j.catena.2014.07.013

Zhang, W., Liu, W., Li, W., Zhu, X., Chen, C., Zeng, H., et al. (2021) Characteristics of throughfall kinetic energy under the banana (*Musa nana* Lour.) canopy: the role of leaf shapes. *Catena*, 197, 104985. Available from: https://doi.org/10.1016/j.catena.2020.104985

Zhongming, W., Lees, B.G., Feng, J., Wanning, L. & Haijing, S. (2010) Stratified vegetation cover index: a new way to assess vegetation impact on soil erosion. *Catena*, 83(1), 87–93. Available from: https://doi.org/10.1016/j.catena.2010.07.006

How to cite this article: Senn, J.A., Schäfer, J., Hosseini, Z. & Seitz, S. (2025) Predicting rainfall kinetic energy under forest canopies—*A pilot study using ULS*. *Earth Surface Processes and Landforms*, 50(11), e70150. Available from: https://doi.org/10.1002/esp.70150

APPENDIX A

TABLE A1 Measured kinetic energy by cup and event (J m^{-2}).

		Timestep					
Cup ID	**Position**	**a**	**b**	**c**	**d**	**e**	**f**
A01	Open	53.49	25.48	105.32	70.57	219.93	72.14
A02	Open	37.30	41.15	123.71	36.86	270.00	55.59
A03	Mid crown	256.61	83.79	835.75	242.34	521.01	283.49
A04	Mid crown	159.17	24.60	864.03	310.98	526.44	365.87
A05	Mid crown understorey	88.86	14.27	347.49	177.90	459.81	222.03
A06	Near stem	118.81	3.06	273.24	237.87	462.88	208.02
A07	Near stem	96.39	12.34	313.43	218.26	515.41	191.65
A08	Near stem	309.40	5.60	468.83	258.54	715.55	240.06
A09	Mid crown	462.44	40.45	1049.90	264.05	693.49	254.95
A10	Mid crown understorey	676.41	18.56	392.14	144.20	531.17	187.88
B01	Open	27.75	15.23	174.05	57.17	262.21	74.07
B02	Open	58.13	36.16	233.93	107.69	267.29	105.15
B03	Mid crown	358.17	78.80	846.87	102.61	559.18	146.12
B04	Mid crown understorey	196.73	32.04	357.99	NA	NA	259.41
B05	Mid crown understorey	221.68	45.61	528.63	235.34	392.58	283.75
B06	Mid crown	NA	9.11	359.39	254.77	628.70	357.03
B07	Mid crown understorey	126.60	9.63	629.14	NA	315.18	334.62
B08	Mid crown understorey	124.93	2.10	605.94	215.55	427.51	218.70
B09	Mid crown understorey	203.12	5.34	322.18	124.06	836.81	114.69
B10	Near stem	110.75	2.98	535.11	240.24	358.34	137.37
C01	Mid crown understorey	229.99	5.43	361.14	320.52	507.44	NA
C02	Mid crown understorey	272.02	37.82	325.16	276.57	597.62	330.68
C03	Mid crown understorey	466.56	39.84	591.66	349.68	733.85	383.91
C04	Mid crown	753.54	52.53	752.49	601.82	983.45	588.69
C05	Mid crown	461.92	118.89	NA	603.13	839.26	584.84
C06	Near stem	594.55	71.27	492.56	668.62	886.71	597.09
C07	Mid crown	366.75	71.35	588.86	501.75	882.42	529.94
C08	Near stem	221.06	28.19	430.75	361.93	755.03	348.45
C09	Near stem	NA	NA	636.84	439.76	944.40	405.62

TABLE A1 (Continued)

		Timestep					
Cup ID	**Position**	**a**	**b**	**c**	**d**	**e**	**f**
D01	Mid crown	588.16	106.46	597.36	521.89	802.75	NA
D02	Mid crown	521.62	49.03	651.99	NA	678.69	NA
D03	Near stem	499.21	90.26	537.21	495.01	672.30	461.92
D04	Near stem	462.35	65.22	922.08	427.16	952.11	452.72
D05	Near stem	545.88	132.29	605.76	461.21	753.63	443.88
D06	Mid crown	543.95	151.20	700.14	511.12	875.24	541.94
D07	Mid crown	461.30	74.59	537.21	495.45	858.61	422.60
D08	Mid crown	332.60	108.56	569.34	NA	NA	NA
D09	Near stem	484.59	69.34	676.85	551.13	913.94	529.77